Appl Biochem Biotechnol (2018) 185:834–846
https://doi.org/10.1007/s12010-018-2701-y

Fabrication of a New Self-assembly Compound of $CsTi_2NbO_7$ with Cationic Cobalt Porphyrin Utilized as an Ascorbic Acid Sensor

Mengjun Wang[1] · **Jiasheng Xu**[1] · **Xiaobo Zhang**[1] · **Zichun Fan**[1] · **Zhiwei Tong**[1,2]

Received: 6 December 2017 / Accepted: 15 January 2018 /
Published online: 23 January 2018

Abstract A novel sandwich-structured nanocomposite based on $Ti_2NbO_7^-$ nanosheets and cobalt porphyrin (CoTMPyP) was fabricated through electrostatic interaction, in which CoTMPyP has been successfully inserted into the lamellar spacing of layered titanoniobate. The resultant Ti_2NbO_7/CoTMPyP nanocomposite was characterized by XRD, SEM, TEM, EDS, FT-IR, and UV-vis. It is demonstrated that the intercalated CoTMPyP molecules were found to be tilted approximately 63° against $Ti_2NbO_7^-$ layers. The glass carbon electrode (GCE) modified by Ti_2NbO_7/CoTMPyP film showed a fine diffusion-controlled electrochemical redox process. Furthermore, the Ti_2NbO_7/CoTMPyP-modified electrode exhibited excellent electrocatalytic oxidation activity of ascorbic acid (AA). Differential pulse voltammetric studies demonstrated that the intercalated nanocomposite detects AA linearly over a

Electronic supplementary material The online version of this article (https://doi.org/10.1007/s12010-018-2701-y) contains supplementary material, which is available to authorized users.

✉ Zhiwei Tong
Tong@hhit.edu.cn

Mengjun Wang
2016210061@hhit.edu.cn

Jiasheng Xu
2015210047@hhit.edu.cn

Xiaobo Zhang
2000000029@hhit.edu.cn

Zichun Fan
2017210108@hhit.edu.cn

[1] School of Chemical Engineering, Huaihai Institute of Technology, Lianyungang 222005, China

[2] SORST, Japan Science and Technology Agency (JST), Kawaguchi Center Building 4-1-8, Kawaguchi-shi, Saitama 332-0012, Japan

concentration range of 4.99×10^{-5} to 9.95×10^{-4} mol L^{-1} with a detection limit of 3.1×10^{-5} mol L^{-1} at a signal-to-noise ratio of 3.0.

Keywords Intercalation · Electrostatic self-assembly · Layered titanoniobate · Cobalt porphyrin · Electrocatalysis

Introduction

In recent years, layered materials with particular structure and properties have attracted tremendous interests in fields of electrochemical and photochemical catalysis [1–7]. As a typical layered metal oxide semiconductor firstly discovered in 1979 [8], layered $CsTi_2NbO_7$ has been widely investigated as electrocatalysts due to its ability of ion exchanging [9], swelling [10], and delaminating to nanosheets [11], favorable charge transfer, and easy modification characters [12–14]. The corresponding crystal structure of $CsTi_2NbO_7$ is shown in Fig. 1; cesium ions (Cs^+) lie between MO_6 (M=Ti, Nb) octahedral layers, which are joined by sharing corner and edge. One of the most remarkable aspects of the exfoliated nanosheets is that they can be used as building blocks for fabricating various nanostructures [15]. However, the drawbacks of pure $CsTi_2NbO_7$ are (i) low electrochemical activity and (ii) small specific surface area. Therefore, it is necessary to take some efficient modifications to enhance electrochemical activity of $CsTi_2NbO_7$.

As we know, water-soluble porphyrins and their derivatives show excellent activities in redox, optics, and electricity [16], which are sensitive to pH and temperature. In our group, metalloporphyrin, such as MnTMPyP and CoTMPyP, has been successfully intercalated into the interlayer spacing of $K_2Ti_4O_9$ [17], $K_4Nb_6O_{17}$ [18, 19], $KLaNb_2O_7$ [20], and KNb_3O_8 [21], showing enhanced electrochemical catalytic activities towards O_2, $NaNO_2$, and H_2O_2. It is noteworthy that layered inorganic matrices with large surface area are really needed for the synthesis of solventless catalysts and have been chosen as a class of preferable material on account of their better stability during the process of electrochemical detection. Therefore, it is feasible to construct a novel nanocomposite by combining metalloporphyrin with $Ti_2NbO_7^-$ nanosheets to solve the abovementioned problems.

Ascorbic acid (AA) is a water-soluble intracellular antioxidant that can directly participate in various biological reactions, and plays an important role in the regulation of the activity of

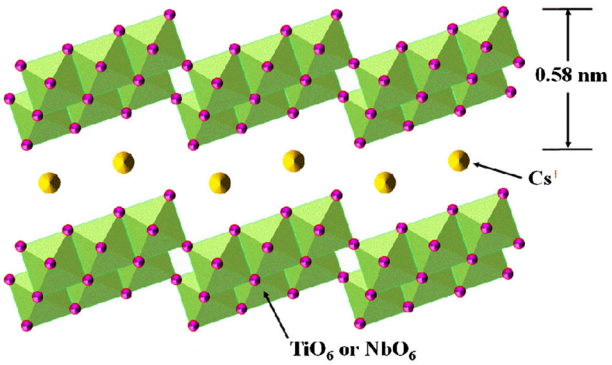

Fig. 1 The crystal structure of $CsTi_2NbO_7$

cellular immunity including synthesizing collagen, remedying scurvy, and preventing arteriosclerosis and cancer [22, 23]. Therefore, the detection of AA has aroused great interests in recent decades. Up to now, various methods including colorimetric method [24], flow injection [25], fluorometric method [26], and electrochemistry [27, 28] have been used to detect it. Among those detection methods, the electrochemical technique has been widely used due to short time and low cost. Recently, there are various porphyrin-based nanocomposites that have been utilized in the electrochemical detection of AA, such as $KLaNb_2O_7$ [20], graphene [29], and carbon nanotubes [30].

In this paper, we have developed a novel sandwich-structured nanocomposite based on $Ti_2NbO_7^-$ nanosheets and cobalt porphyrin (CoTMPyP). The resultant Ti_2NbO_7/CoTMPyP composite was detailed and characterized by X-ray powder diffraction (XRD), scanning electron micrograph (SEM), transmission electron microscope (TEM), energy-dispersive spectroscopy (EDS), Fourier transform infrared (FTIR), and UV-vis. Furthermore, the electrocatalytic oxidation of AA on Ti_2NbO_7/CoTMPyP-modified electrode was studied via cyclic voltammetry (CV) and differential pulse voltammetry (DPV) analysis technologies.

Experimental Details

Exfoliation of $Ti_2NbO_7^-$ Nanosheets

The detailed preparation process for Ti_2NbO_7/CoTMPyP composite was shown in Fig. 2. Layered $CsTi_2NbO_7$ was synthesized by calcinating the mixture of Cs_2CO_3, TiO_2, and Nb_2O_5 with the molar ratios of 1.1:4:1 and continuously heated at 750, 950, and 1050 °C for 12 h at each temperature [10]. The protonated form of HTi_2NbO_7 was obtained by treating $CsTi_2NbO_7$ with 2 mol L^{-1} HCl for 3 days at room temperature, and the acid was exchanged each day to ensure proton reaction. Then, 0.05 g HTi_2NbO_7 was dispersed in 20 mL distilled water, and then 430 μL TBAOH aqueous solution (10 wt%) was added under vigorous stirring for 4 days. The resultant subtransparent colloidal solution was centrifuged at 4000 rpm for 10 min to remove unexfoliated particles.

Fabrication of Ti_2NbO_7/CoTMPyP Composite

To prepare Ti_2NbO_7/CoTMPyP composite, 1 mmol L^{-1} CoTMPyP aqueous solution was added dropwise into $Ti_2NbO_7^-$ nanosheet colloidal solution with an appropriate volume ratio (CoTMPyP: $Ti_2NbO_7^- = 1:1$). After hours, the flocculated precipitate was centrifuged (8000 rpm) and washed with distilled water for three times. The product was dried at 50 °C in a vacuum oven overnight.

Apparatus

X-ray diffraction patterns of the resulted samples were carried out with a RINT 2000 diffractometer (Rigaku) using Cu Kα radiation ($\lambda = 0.154$ nm) with 2θ ranging from 1.5° to 60° at a scan rate of 1°/min. The scanning electron micrograph (SEM) images were collected by a JSM-5600 apparatus (JEOL) operating at 15 kV for the Au-coated samples. The TEM images were obtained by a Philips Tecnai 12 transmission electron microscope operating at 120 kV. The EDS analysis was performed on a FEI Tecnai G2F30S-TWIN high-resolution

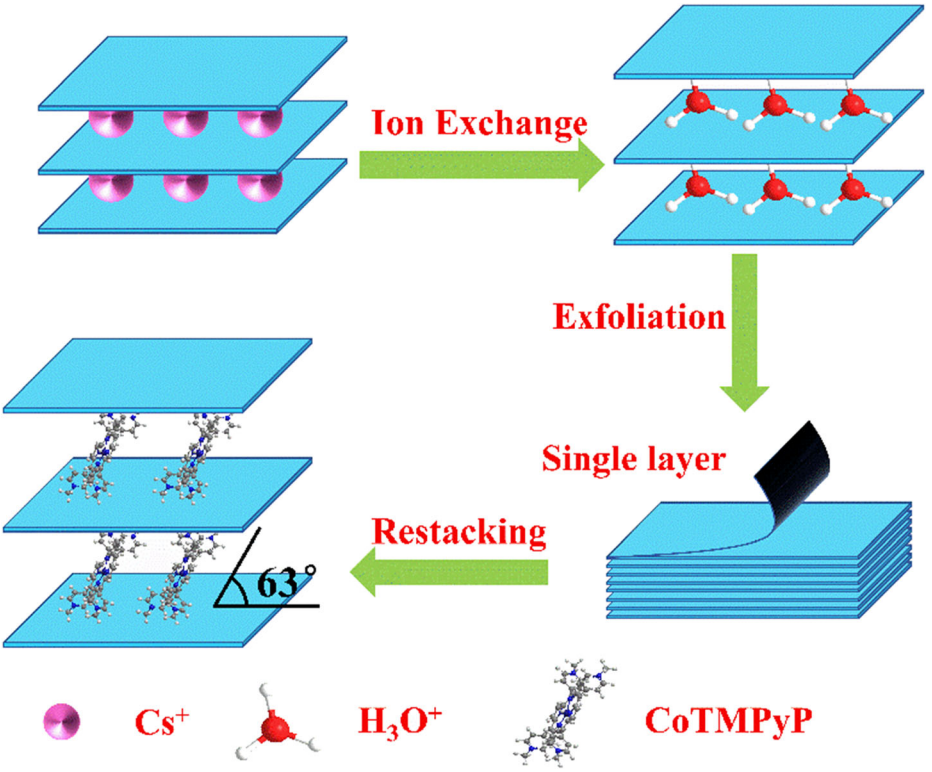

Fig. 2 Schematic illustration of the self-assembly process of Ti_2NbO_7/CoTMPyP nanocomposite

transmission electron microscope. The atomic force microscope (AFM) images were taken with a Bruker dimension edge SPM apparatus. FTIR spectra were measured on a Shimadzu FTIR-8400S apparatus spectrometer with KBr pellets. UV-vis absorption spectra were recorded using a UV-vis spectrometer (UV-2550). Zeta potential of $Ti_2NbO_7^-$ colloidal solution was collected by a Malvern Zetasizer Nano instrument. Electrochemical measurements were performed with a three-electrode electrochemical cell in a CHI660E electrochemical workstation, with a saturated calomel electrode (SCE) as the reference electrode, a platinum wire as the counter electrode, and a glass carbon electrode (GCE) coated by the Ti_2NbO_7/CoTMPyP hybrid as the working electrode.

Results and Discussion

Characterization of Ti_2NbO_7/CoTMPyP Nanocomposite

The XRD pattern of $CsTi_2NbO_7$ has a characteristic peak at 9.62° (Fig. 3a), corresponding to (020) of JCPDS Card No. 73-0680, matching well with the diffraction peaks as previously reported [12]. After the proton exchange reaction, the (020) peak shifts from 9.62° to 8.36° due to the exchange of Cs^+ to H_3O^+. By combination of $Ti_2NbO_7^-$ nanosheets with CoTMPyP, (020) peak of the resulted Ti_2NbO_7/CoTMPyP was changed to 4.06°, demonstrating the successful intercalation of metalloporphyrin molecule into Ti_2NbO_7 layers. In addition, it

was confirmed that different volume ratios of Ti_2NbO_7 and CoTMPyP have no effect on the arrangement of Ti_2NbO_7/CoTMPyP nanocomposite (Fig. S1). The basal spacing and Δd values of products are listed in Table 1. Since the basal spacing of host $CsTi_2NbO_7$ is 0.92 nm, the thickness of the single $Ti_2NbO_7^-$ layer can be calculated as 0.58 nm by subtracting the diameter of Cs^+ (about 0.338 nm) [31], and the net interlayer height of Ti_2NbO_7/CoTMPyP can be calculated as 1.59 nm. In consideration of the molecular dimension of CoTMPyP (1.8 nm × 1.8 nm × 0.75 nm, estimated by MM2 calculation) [20], the arrangement of CoTMPyP molecular between the interlayers of $Ti_2NbO_7^-$ nanosheets can be inferred as a tilted monolayer and its inserting angle is approximately 63° (Fig. 4).

The SEM images of the resulted samples were shown in Fig. 5. The SEM image of the host $CsTi_2NbO_7$ is compact, with a typical layered structure (Fig. 5a). After proton reaction, the obtained HTi_2NbO_7 remains the two-dimension laminar appearance (Fig. 5b), and then through exfoliation/restacking process, the resultant Ti_2NbO_7/CoTMPyP was arranged with stratified structure (Fig. 5c). In an effort to assess the size and thickness of $Ti_2NbO_7^-$ nanosheets, the diluted exfoliated solution sample was dripped on the mica plate where AFM imaging was performed at multiple locations across the sample. As shown in Fig. 5d, e, the $Ti_2NbO_7^-$ nanosheet possesses an unilaminar morphology with its surface distance of approximately hundreds of nanometers and vertical distance of 1.08 nm, in line with the results reported in previous literature [15]. In comparison with the thickness calculated by XRD data, the thicker nanosheets may be owing to the existence of H_3O^+ molecule on the surface of nanosheets.

The FT-IR spectra of $CsTi_2NbO_7$, CoTMPyP, and Ti_2NbO_7/CoTMPyP were shown in Fig. 6a. For CoTMPyP, a peak at 1640 cm^{-1} can be ascribed to the stretching vibration of C=N in the pyridine substituent group, while those at 1510, 1410, and 1090 cm^{-1} are assigned to the stretching vibration of C=N, C=C, and C-N in porphyrin rings, respectively. The bands at region from 1000 to 400 cm^{-1} are characteristic peaks of Ti-O and Nb-O stretching vibration in $CsTi_2NbO_7$. After combining CoTMPyP with Ti_2NbO_7 nanosheets, the characteristic peaks of CoTMPyP were also observed with a shift in the resulted Ti_2NbO_7/CoTMPyP composite. It indicates that there is a strong interaction between CoTMPyP with Ti_2NbO_7 nanosheets.

UV-vis optical spectra of CoTMPyP and Ti_2NbO_7/CoTMPyP nanocomposite were shown in Fig. 6b. The CoTMPyP aqueous solution (Fig. 6b (a)) has a Soret band and a *Q* band in 437 and 550 nm, respectively. There are 18 and 13 nm red shifts in Soret and *Q* band after intercalation. Besides, the two broaden absorption bands in Ti_2NbO_7/CoTMPyP are probably caused by the effect of steric hindrance of immobilizing CoTMPyP molecule between

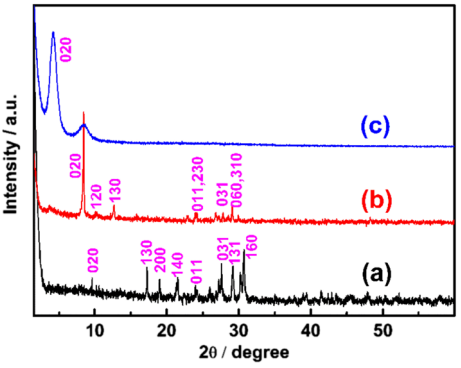

Fig. 3 XRD patterns of (a) $CsTi_2NbO_7$, (b) HTi_2NbO_7, and (c) Ti_2NbO_7/CoTMPyP

Table 1 XRD data of the different samples

Compound	*d*/nm	Δ*d*/nm
$CsTi_2NbO_7$	0.92	
HTi_2NbO_7	1.06	0.48
$CoTMPyP/Ti_2NbO_7$	2.17	1.59

Δd basal spacing-layer thickness (0.58 nm)

Ti_2NbO_7 layers. There are numerous similar situations reported in the recent years [32, 33]; some of them speculate that a certain degree of superposing and reuniting of metalloporphyrin molecules may result in these phenomena [34]. These results confirmed a strong intercalation of CoTMPyP molecules into $Ti_2NbO_7^-$ nanosheets.

The zeta potential analysis was carried out to study the driving force of the exfoliation/restacking process. As is shown in Fig. S2, tyndall phenomenon can be observed in the exfoliated colloidal suspension with a zeta potential of − 41.8 mV, which expresses the colloid is in a stable and well-disseminated condition. When CoTMPyP aqueous solution was added into $Ti_2NbO_7^-$ nanosheets, the potential of $Ti_2NbO_7^-$ nanosheets increased gradually, accompanied with a large number of flocculent precipitates (Fig. 7). It shows that the exfoliation/restacking approach is unique as it not only exhibits excellent time-saving advantage but also makes the best use of high specific surface area of $Ti_2NbO_7^-$ nanosheets. When the volume ratio of CoTMPyP aqueous solution and $Ti_2NbO_7^-$ nanosheets was 0.65, the potential value tends to be zero. Furthermore, the potential value changed towards positive by a continuous addition of CoTMPyP into $Ti_2NbO_7^-$ nanosheets. It can be inferred that the recombination process of Ti_2NbO_7/CoTMPyP nanocomposite is based on electrostatic force.

In order to certify the combination of $Ti_2NbO_7^-$ nanosheets and CoTMPyP, EDS analysis was performed via dropping the dispersion liquid of Ti_2NbO_7/CoTMPyP nanocomposite on copper wire mesh. Figure S3 indicates the presence of C, N, O, Ti, Nb, and Co elements in the nanocomposite. Furthermore, Ca signal comes from the ultrapure water.

Electrochemical Behavior of Ti_2NbO_7/CoTMPyP Nanocomposite Thin Film

Based on the above combined results, it can be concluded that Ti_2NbO_7/CoTMPyP nanocomposite was successfully fabricated through electrostatic self-assembly method. Then, cyclic voltammetry (CV) and differential pulse voltammetry (DPV) analysis technologies were measured to further study the electrocatalytic performance of this hybrid film. Firstly, it is necessary to understand the role of $Ti_2NbO_7^-$ matrix during a redox process. Figure 8a gives a comparison of electrochemical behaviors between CoTMPyP aqueous solution and Ti_2NbO_7/CoTMPyP-modified electrode in N_2-saturated 0.2 mol L^{-1} and pH 7.0 PBS at a scan rate of

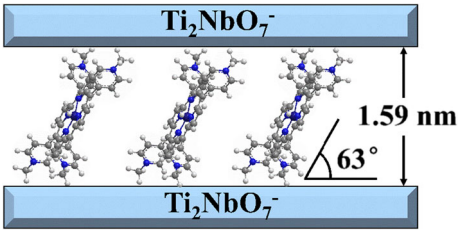

Fig. 4 Proposed possible arrangement of CoTMPyP molecules between the Ti_2NbO_7 nanosheets

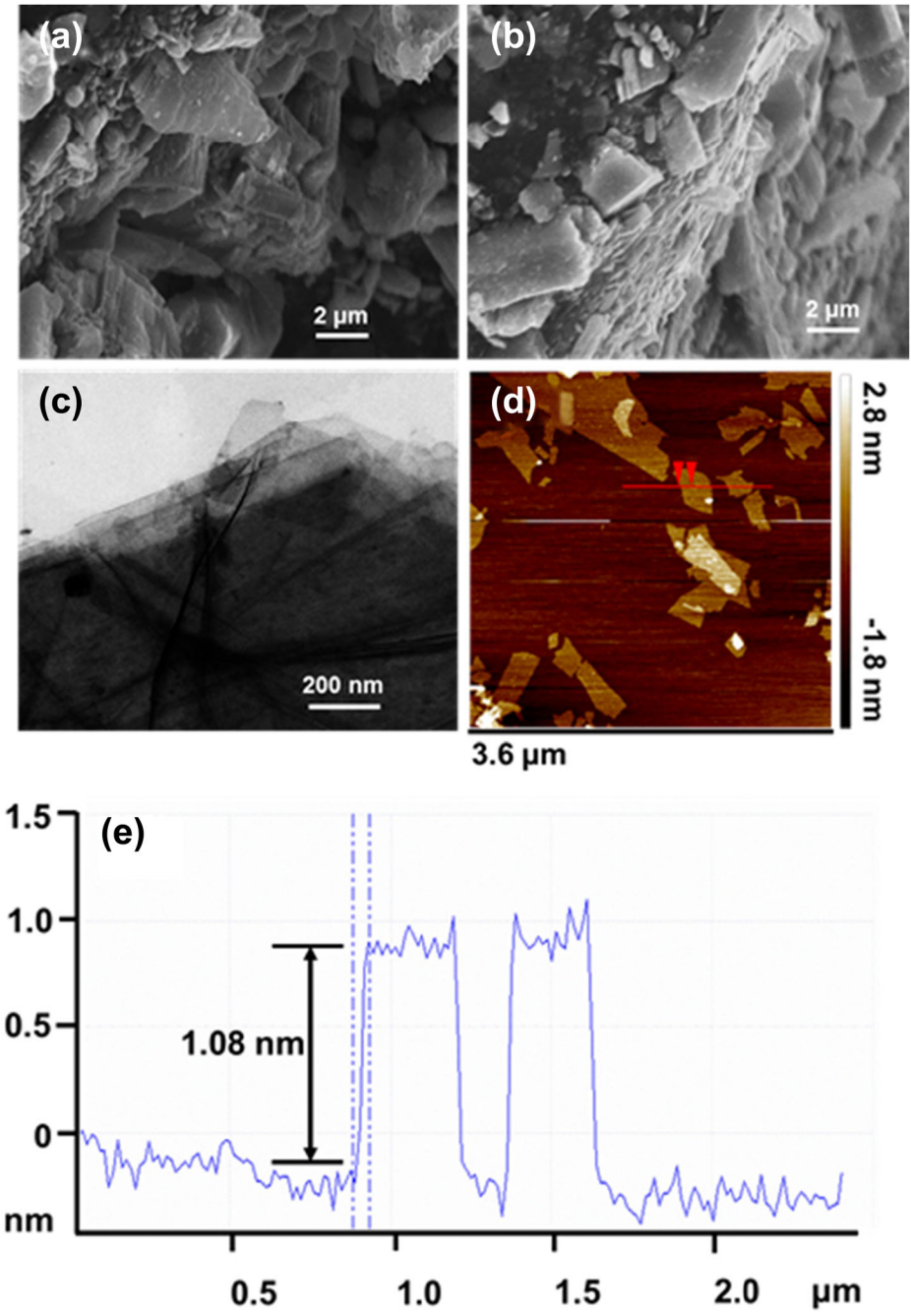

Fig. 5 SEM images of **a** $CsTi_2NbO_7$ and **b** HTi_2NbO_7. **c** TEM image of Ti_2NbO_7/CoTMPyP. **d** AFM images of Ti_2NbO_7 nanosheets. **e** Nanoscope analysis of Ti_2NbO_7 nanosheets

100 mV s^{-1}. There are two pairs of redox peaks for CoTMPyP aqueous solution; the reduction potentials are located at −0.751 and −0.953 V, corresponding to $Co^{II/I}$TMPyP and $Co^{III/}$

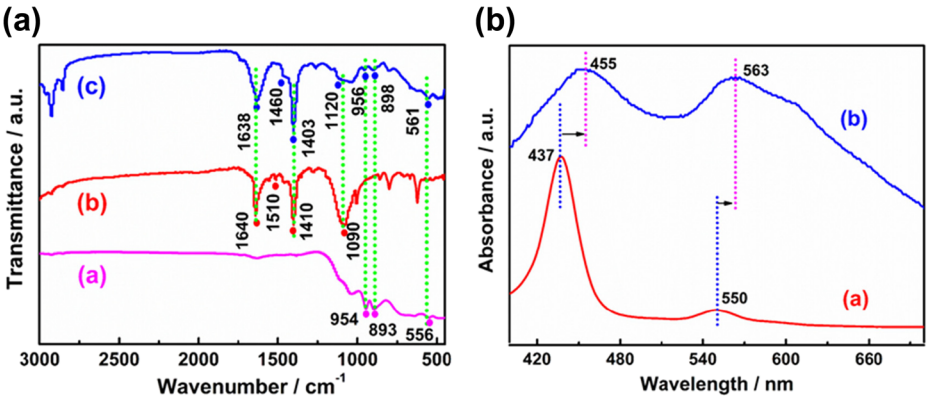

Fig. 6 **a** FT-IR spectra of (a) $CsTi_2NbO_7$, (b) CoTMPyP, and (c) Ti_2NbO_7/CoTMPyP. **b** UV-vis absorption spectra of (a) CoTMPyP aqueous solution and (b) Ti_2NbO_7/CoTMPyP

^{II}TMPyP redox couple, respectively [35]. While the redox peaks for Ti_2NbO_7/CoTMPyP-modified electrode appear at −0.745 and −0.969 V, it is obvious that the potential of $Co^{III/II}$TMPyP redox couple turns negative accompanied with a clear increase in current, indicating that the Ti_2NbO_7 inorganic matrix in the nanocomposite can promote the movement of charge in the electrochemical process [36]. The reasons for the superior electrochemical performances of Ti_2NbO_7/CoTMPyP nanocomposite may derive from the truth that the layered Ti_2NbO_7 provides a two-dimensional channel and acts as an electron transporter during the process.

Secondly, in this paper, ascorbic acid was chosen for testing the electrochemical oxidation abilities towards chemical species on the surface of Ti_2NbO_7/CoTMPyP-modified electrode. To begin with, a comparison between bare electrode and modified electrode has been implemented. The CV curves were conducted in N_2-saturated 0.2 mol L^{-1} and pH 7.0 PBS containing 8 mmol L^{-1} AA at a scan rate of 50 mV s^{-1}. As is shown in Fig. 8b, there is a strong oxidation process of AA; however, the coupled cathodic signal is absent in the reverse scan. This phenomenon is caused by the irreversible electron transfer process. In previous studies, it has been proved that when the oxidation process of ascorbic acid proceeds in pH < 8 condition, the existence of two successive one electron oxidation steps accompanied by rapid dehydration leads to irreversibility [37–39]. Obviously, the oxidation peak potential for bare electrode is around 0.28 V, while for Ti_2NbO_7/CoTMPyP-modified electrode, the oxidation potential shifts negatively towards 0.041 V and the oxidation peak current increases remarkably. It really

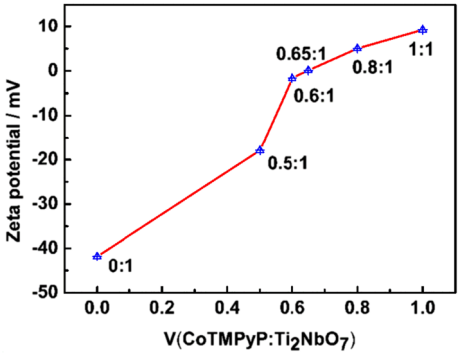

Fig. 7 The relationship between zeta potential and CoTMPyP/$Ti_2NbO_7^-$ volume ratio

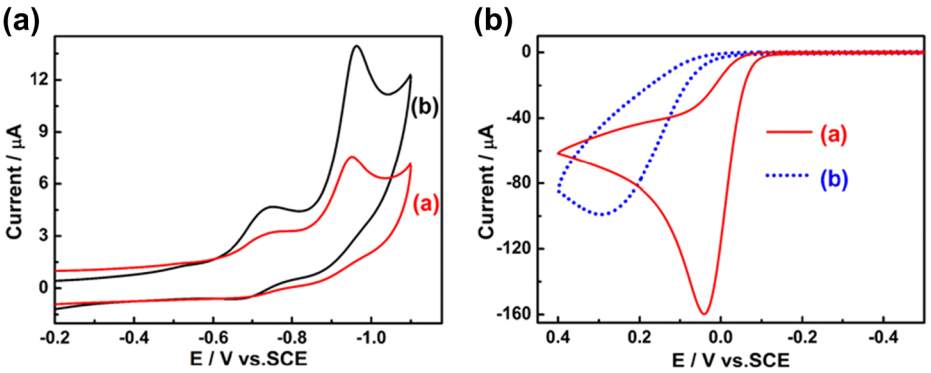

Fig. 8 **a** CV curves of (a) CoTMPyP aqueous solution and (b) Ti_2NbO_7/CoTMPyP-modified electrode in N_2-saturated 0.2 mol L^{-1} and pH 7.0 PBS at a scan rate of 100 mV s^{-1}. **b** CV curves of (a) Ti_2NbO_7/CoTMPyP-modified electrode (solid line) and (b) bare electrode (dash line) in N_2-saturated 0.2 mol L^{-1} and pH 7.0 PBS containing 8 mmol L^{-1} AA at a scan rate of 50 mV s^{-1}

indicates that the Ti_2NbO_7/CoTMPyP nanocomposite has promoted the electron transfer reaction of AA. For this reason, there is no doubt that Ti_2NbO_7/CoTMPyP nanocomposite is an excellent catalyst for electrochemical oxidation towards AA.

In addition, the influence of scan rates was examined. In Fig. 9a, with the improvement of scan rates, the oxidation peak current increases gradually and the oxidation peak potential turns positively; this may be also attributed to the irreversibility of AA oxidation [36]. Furthermore, as we can see in Fig. 9b, there is a good linear relationship between square root of scan rate ($v^{1/2}$) and oxidation peak current (I_{pa}). The linear equation can be expressed as $I_{pa} = -47.65 - 15.65\ v^{1/2}$, $|R| = 0.9993$, so it can be speculated that the electrochemical oxidation process towards AA on the modified electrode is diffusion-controlled. What's more, according to related literatures [40–42], the mechanism of electrocatalytic oxidation of ascorbic acid on the modified electrode can be proposed as follows:

$$H_2A \rightarrow HA^- + H^+ \tag{1}$$

$$Co^{III}TMPyP + HA^- \rightarrow Co^{II}TMPyP\bullet\bullet\bullet A^{\bullet -} + H^+ \tag{2}$$

$$Co^{II}TMPyP\bullet\bullet\bullet A^{\bullet -} \rightarrow Co^{II}TMPyP + A + e^- \tag{3}$$

$$Co^{II}TMPyP \rightarrow Co^{III}TMPyP + e^- \tag{4}$$

$$\textit{The total reaction is } H_2A \rightarrow A + 2H^+ + 2e^- \tag{5}$$

The controlling step of this process is the migration of HA^- towards the modified electrode surface, namely rate-determining step.

Thirdly, differential pulse voltammetry (DPV) analysis technology was utilized for accurate electrochemical determination of AA (Fig. 9c). The relationship between AA concentration (C) and peak current (I_{pa}) was given in Fig. 9d, and the linear equation can be expressed as

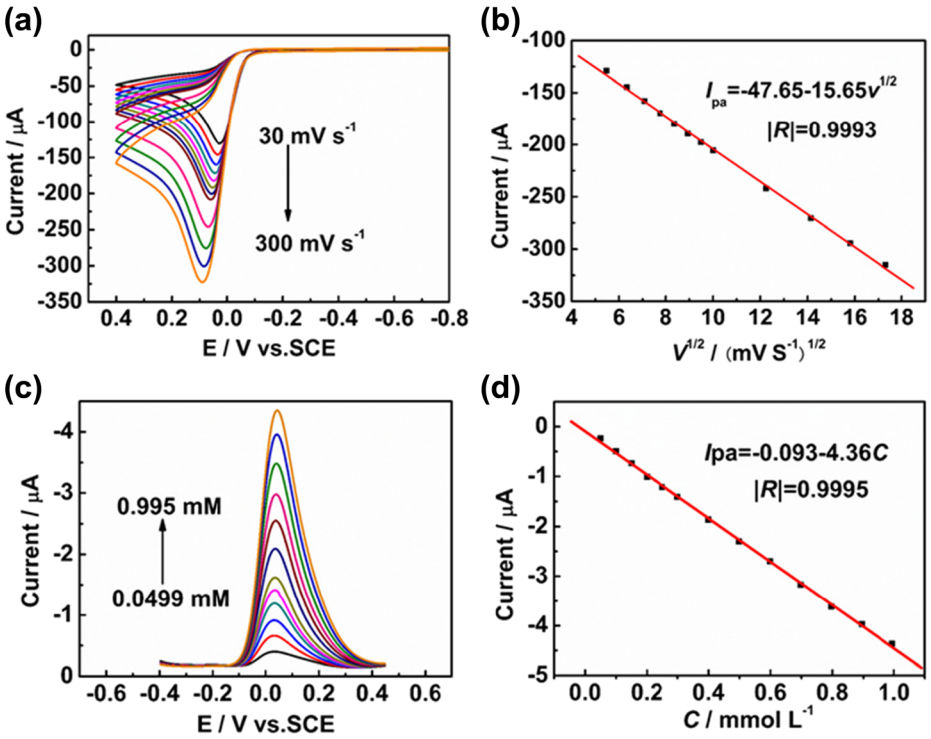

Fig. 9 **a** CV curves of Ti_2NbO_7/CoTMPyP-modified electrode in N_2-saturated 0.2 mol L^{-1} and pH 7.0 PBS containing 8 mmol L^{-1} AA at a scan rate of 30, 40, 50, 60, 70, 80, 90, 100, 150, 200, 250, and 300 mV s^{-1}, respectively. **b** The relationship curve between the oxidation peak current (I_{pa}) and the square root of scan rate ($v^{1/2}$). **c** DPV curves of Ti_2NbO_7/CoTMPyP-modified electrode in N_2-saturated 0.2 mol L^{-1} and pH 7.0 PBS with different concentrations of AA. **d** The relationship between AA concentration (C) and peak current (I_{pa})

$I_{pa} = -0.093 - 4.36\ C$ (mmol L^{-1}) ($|R| = 0.9995$) with a detection range of 4.99×10^{-5} to 9.95×10^{-4} mol L^{-1}. A detection limit of 3.1×10^{-5} mol L^{-1} can be calculated at a signal-to-noise ratio of 3.0. These results confirm that the sensitivity of Ti_2NbO_7/CoTMPyP towards ascorbic acid detection is comparable with other reported modified electrodes (Table S1).

Last but not least, in order to investigate the stability of Ti_2NbO_7/CoTMPyP-modified electrode, the CVs and DPVs for 0.25 mmol L^{-1} ascorbic acid in 0.2 mol L^{-1} and pH 7.0 PBS were recorded for every 2 min (Figs. S4 and S5). It was found that the oxidation peak current and potential remained almost the same with the relative standard deviation (RSD) of 0.38% for CVs and 0.25% for DPVs. In addition, to ascertain the reproducibility of the results, Ti_2NbO_7/CoTMPyP hybrid was coated on two different electrodes and stored at room temperature for a month; the RSD was only 0.78% (Fig. S6). All these observations indicate that Ti_2NbO_7/CoTMPyP nanocomposite has satisfactory stability, reproducibility, and repeatability.

Conclusion

A facile and rapid electrostatic self-assembly technique was used for the combination of $Ti_2NbO_7^-$ nanosheets and CoTMPyP cations for the first time. The size and thickness of $Ti_2NbO_7^-$ nanosheets were confirmed by AFM. Besides, the zeta potential of exfoliated

nanosheets was − 41.8 mV, suggesting the colloidal solution was in a stable and well-dispersed condition. In addition, the Ti_2NbO_7/CoTMPyP nanocomposite with outstanding stability and reproducibility exhibits excellent electrochemical catalytic ability towards ascorbic acid in pH 7.0 PBS, and a detection limit was calculated as 3.1×10^{-5} mol L^{-1} by DPV analysis. In summary, this research offers a convenient method for the development of $CsTi_2NbO_7$-based lamellar nanocomposites, and it can be pointed out that the Ti_2NbO_7/CoTMPyP nanocomposite is a promising material in constructing ascorbic acid biosensors.

Funding Information This work was supported by Natural Science Fund of Jiangsu Province (BK20161294), HHIT Research Project (Z2015011), Lianyungang Science Project (CG1602), and the Natural Science Foundation of Huaihai Institute of Technology (Z2014004).

Compliance with Ethical Standards

Conflict of Interest The authors declare that they have no conflict of interest.

References

1. Liu, X., Wei, S., Chen, S., Yuan, D., & Zhang, W. (2014). Graphene-multiwall carbon nanotube-gold nanocluster composites modified electrode for the simultaneous determination of ascorbic acid, dopamine, and uric acid. *Applied Biochemistry and Biotechnology, 173*(7), 1717–1726. https://doi.org/10.1007/s12010-014-0959-2
2. Liu, C., Han, R., Ji, H., Sun, T., Zhao, J., Chen, N., Chen, J., Guo, X., Hou, W., & Ding, W. (2016). S-doped mesoporous nanocomposite of $HTiNbO_5$ nanosheets and TiO_2 nanoparticles with enhanced visible light photocatalytic activity. *Physical Chemistry Chemical Physics, 18*(2), 801–810. https://doi.org/10.1039/C5CP06555K
3. Zhang, X., Li, D., Yin, F., Gong, J., Yang, X., Tong, Z., & Xu, X. (2014). Characterization of a layered methylene blue/vanadium oxide nanocomposite and its application in a reagentless H_2O_2 biosensor. *Applied Biochemistry and Biotechnology, 172*(1), 176–187. https://doi.org/10.1007/s12010-013-0528-0
4. Zhai, Z., Hu, C., Yang, X., Zhang, L., Liu, C., Fan, Y., & Hou, W. (2012). Nitrogen-doped mesoporous nanohybrids of TiO_2 nanoparticles and $HTiNbO_5$ nanosheets with a high visible-light photocatalytic activity and a good biocompatibility. *Journal of Materials Chemistry, 22*(36), 19122–19131. https://doi.org/10.1039/c2jm32338a
5. Zhai, Z., Huang, Y., Xu, L., Yang, X., Hu, C., Zhang, L., Fan, Y., & Hou, W. (2011). Thermostable nitrogen-doped $HTiNbO_5$ nanosheets with a high visible-light photocatalytic activity. *Nano Research, 4*(7), 635–647. https://doi.org/10.1007/s12274-011-0119-8
6. Liu, C., Sun, T., Wu, L., Liang, J., Huang, Q., Chen, J., & Hou, W. (2015). N-doped $Na_2Ti_6O_{13}$@TiO_2 core–shell nanobelts with exposed {1 0 1} anatase facets and enhanced visible light photocatalytic performance. *Applied Catalysis B, 170*, 17–24.
7. Zhai, Z., Yang, X., Xu, L., Hu, C., Zhang, L., Hou, W., & Fan, Y. (2012). Novel mesoporous NiO/$HTiNbO_5$ nanohybrids with high visible-light photocatalytic activity and good biocompatibility. *Nanoscale, 4*(2), 547–556. https://doi.org/10.1039/C1NR11091H
8. Hervieu, M., & Raveau, B. (1980). A layer structure: the titanoniobate $CsTi_2NbO_7$. *Journal of Solid State Chemistry, 32*(2), 161–165. https://doi.org/10.1016/0022-4596(80)90562-9
9. Rebbah, H., Hervieu, M., & Raveau, B. (1981). The $CsTi_2NbO_7$ type layer oxides: ion exchange properties. *Materials Research Bulletin, 16*(2), 149–157. https://doi.org/10.1016/0025-5408(81)90075-1
10. Dias, A. S., Lima, S., Carriazo, D., Rives, V., Pillinger, M., & Valente, A. A. (2006). Exfoliated titanate, niobate and titanoniobate nanosheets as solid acid catalysts for the liquid-phase dehydration of D-xylose into furfural. *Journal of Catalysis, 244*(2), 230–237. https://doi.org/10.1016/j.jcat.2006.09.010
11. Akatsuka, K., Takanashi, G., Ebina, Y., Haga, M. A., & Sasaki, T. (2012). Electronic band structure of exfoliated titanium-and/or niobium-based oxide nanosheets probed by electrochemical and photoelectrochemical measurements. *The Journal of Physical Chemistry C, 116*(23), 12426–12433. https://doi.org/10.1021/jp302417a

12. Xie, K., Wei, W., & Yu, H. (2016). A novel layered titanoniobate as anode material for long-life sodium-ion batteries. *RSC Advances, 6*(42), 35746–35750. https://doi.org/10.1039/C6RA02530G
13. Catti, M., Pinus, I., Ruffo, R., Salamone, M. M., & Mari, C. M. (2016). A novel layered lithium niobium titanate as battery anode material: crystal structure and charge-discharge properties. *Solid State Ionics, 295*, 72–77. https://doi.org/10.1016/j.ssi.2016.08.001
14. Takagaki, A., Yoshida, T., Lu, D., Kondo, J. N., Hara, M., Domen, K., & Hayashi, S. (2004). Titanium niobate and titanium tantalate nanosheets as strong solid acid catalysts. *Journal of Physical Chemistry B, 108*(31), 11549–11555. https://doi.org/10.1021/jp049170e
15. Tanaka, T., Fukuda, K., Ebina, Y., Takada, K., & Sasaki, T. (2004). Highly organized self-assembled monolayer and multilayer films of titania nanosheets. *Advanced Materials, 16*(11), 872–875. https://doi.org/10.1002/adma.200306470
16. Liu, L., Ma, J., Shao, F., Zhang, D., Gong, J., & Tong, Z. (2012). A nanostructured hybrid synthesized by the intercalation of CoTMPyP into layered titanate: direct electrochemistry and electrocatalysis. *Electrochemistry Communications, 24*, 74–77. https://doi.org/10.1016/j.elecom.2012.08.021
17. Ma, J., Yang, M., Chen, Y., Liu, L., Zhang, X., Wang, M., Zhang, D., & Tong, Z. (2015). Sandwich-structured composite from the direct coassembly of layered titanate nanosheets and Mn porphyrin and its electrocatalytic performance for nitrite oxidation. *Materials Letters, 150*, 122–125. https://doi.org/10.1016/j.matlet.2015.03.039
18. Ma, J., Wu, J., Gu, J., Liu, L., Zhang, D., Xu, X., Yang, X., & Tong, Z. (2012). Fabrication and spectroscopic, electrochemical, and catalytic properties of a new intercalation compound of $K_4Nb_6O_{17}$ with cationic cobalt porphyrin. *Journal of Molecular Catalysis A: Chemical, 357*, 95–100. https://doi.org/10.1016/j.molcata.2012.01.025
19. Ma, J., Wu, J., Zheng, J., Liu, L., Zhang, D., Xu, X., Yang, X., & Tong, Z. (2012). Synthesis, characterization and electrochemical behavior of cationic iron porphyrin intercalated into layered niobate. *Microporous and Mesoporous Materials, 151*, 325–329. https://doi.org/10.1016/j.micromeso.2011.10.016
20. Pan, B., Zhao, W., Zhang, X., Li, J., Xu, J., Ma, J., Liu, L., Zhang, D., & Tong, Z. (2016). Research on self-assembly of exfoliated perovskite nanosheets ($LaNb_2O_7^-$) and cobalt porphyrin utilized for electrocatalytic oxidation of ascorbic acid. *RSC Advances, 6*(52), 46388–46393. https://doi.org/10.1039/C6RA06429A
21. Zhang, X., Liu, L., Ma, J., Yang, X., Xu, X., & Tong, Z. (2013). A novel metalloporphyrin intercalated layered niobate as an electrode modified material for detection of hydrogen peroxide. *Materials Letters, 95*, 21–24. https://doi.org/10.1016/j.matlet.2012.12.061
22. Barnes, M. J. (1975). Function of ascorbic acid in collagen metabolism. *Annals of the New York Academy of Sciences, 258*(1 Second Confer), 264–277. https://doi.org/10.1111/j.1749-6632.1975.tb29287.x
23. Smith, A. R., Visioli, F., & Hagen, T. M. (2002). Vitamin C matters: increased oxidative stress in cultured human aortic endothelial cells without supplemental ascorbic acid. *FASEB Journal, 16*(9), 1102–1104. https://doi.org/10.1096/fj.01-0825fje
24. Kyaw, A. (1978). A simple colorimetric method for ascorbic acid determination in blood plasma. *Clinica Chimica Acta, 86*(2), 153–157. https://doi.org/10.1016/0009-8981(78)90128-6
25. Marques, I. D. H. C., Marques, E. T. A., Silva, A. C., Ledingham, W. M., Melo, E. H. M., Da Silva, V. L., & Lima Filho, J. L. (1994). Ascorbic acid determination in biological fluids using ascorbate oxidase immobilized on alkylamine glass beads in a flow injection potentiometric system. *Applied Biochemistry and Biotechnology, 44*(1), 81–89. https://doi.org/10.1007/BF02921853
26. Speek, A. J., Schrijver, J., & Schreurs, W. H. P. (1984). Fluorometric determination of total vitamin C in whole blood by high-performance liquid chromatography with pre-column derive atization. *Journal of Chromatography, 305*, 53–60. https://doi.org/10.1016/S0378-4347(00)83313-7
27. Sun, C., Lee, H., Yang, J., & Wu, C. (2011). The simultaneous electrochemical detection of ascorbic acid, dopamine, and uric acid using graphene/size-selected Pt nanocomposites. *Biosensors and Bioelectronics, 26*(8), 3450–3455. https://doi.org/10.1016/j.bios.2011.01.023
28. Pournaghi-Azar, M. H., Razmi-Nerbin, H., & Hafezi, B. (2002). Amperometric determination of ascorbic acid in real samples using an aluminum electrode, modified with nickel hexacyanoferrate films by simple electroless dipping method. *Electroanalysis, 14*(3), 206–212. https://doi.org/10.1002/1521-4109(200202)14:3<206::AID-ELAN206>3.0.CO;2-M
29. Deng, K., Zhou, J., & Li, X. (2013). Noncovalent nanohybrid of cobalt tetraphenylporphyrin with graphene for simultaneous detection of ascorbic acid, dopamine, and uric acid. *Electrochimica Acta, 114*, 341–346. https://doi.org/10.1016/j.electacta.2013.09.164
30. Liu, X., Wei, S., Chen, S., Yuan, D., & Zhang, W. (2014). Graphene-multiwall carbon nanotube-gold nanocluster composites modified electrode for the simultaneous determination of ascorbic acid, dopamine, and uric acid. *Applied Biochemistry and Biotechnology, 173*(7), 1717–1726. https://doi.org/10.1007/s12010-014-0959-2
31. Vance Jr., T. B., & Seff, K. (1975). Hydrated and dehydrated crystal structures of seven-twelfths cesium-exchanged zeolite a. *Journal of Physical Chemistry, 79*, 2163–2167.

32. Yao, K., Nishimura, S., Imai, Y., Wang, H., Ma, T., Abe, E., Tateyama, H., & Yamagishi, A. (2003). Spectroscopic and photoelectrochemical study of sensitized layered niobate $K_4Nb_6O_{17}$. *Langmuir, 19*(2), 321–325. https://doi.org/10.1021/la026065s
33. Machado, A. M., Wypych, F., Drechsel, S. M., & Nakagaki, S. (2002). Study of the catalytic behavior of montmorillonite/iron (III) and Mn (III) cationic porphyrins. *Journal of Colloid and Interface Science, 254*(1), 158–164. https://doi.org/10.1006/jcis.2002.8488
34. Halma, M., de Freitas Castro, K. A. D., Taviot-Gueho, C., Prévot, V., Forano, C., Wypych, F., & Nakagaki, S. (2008). Synthesis, characterization, and catalytic activity of anionic iron (III) porphyrins intercalated into layered double hydroxides. *Journal of Catalysis, 257*(2), 233–243. https://doi.org/10.1016/j.jcat.2008.04.026
35. Chen, S., & Chiu, S. (2001). The catalytic and photocatalytic autoxidation of S_x^{2-} to SO_4^{2-} by water-soluble cobalt porphyrin. *Journal of Molecular Catalysis A: Chemical, 166*(2), 243–253. https://doi.org/10.1016/S1381-1169(00)00471-4
36. Ma, J., Jiang, H., Zhuo, N., Li, J., Lu, J., Gong, J., Xu, X., & Tong, Z. (2011). Fabrication of polypyrrole/layered niobate nanocomposite and its electrochemical behavior. *Journal of Materials Science, 46*(21), 6883–6888. https://doi.org/10.1007/s10853-011-5652-z
37. Pisoschi, A. M., Pop, A., Serban, A. I., & Fafaneata, C. (2014). Electrochemical methods for ascorbic acid determination. *Electrochimica Acta, 121*, 443–460. https://doi.org/10.1016/j.electacta.2013.12.127
38. Sternson, A. W., McCreery, R., Feinberg, B., & Adans, R. N. (1973). Electrochemical studies of adrenergic neurotrans-mitters and related compounds. *Journal of Electroanalytical Chemistry and Interfacial Electrochemistry, 46*(2), 313–321. https://doi.org/10.1016/S0022-0728(73)80139-1
39. Rusling, J. F., & Zuman, P. (1980). Effects of buffers on polarographic reduction of pyridinecarboxaldehydes. *Analytical Chemistry, 52*(13), 2209–2211. https://doi.org/10.1021/ac50063a049
40. Qu, F., Li, N., & Jiang, Y. (1998). Electrochemical studies of NiTMPyP and interaction with DNA. *Talanta, 45*(5), 787–793. https://doi.org/10.1016/S0039-9140(97)00154-9
41. Harris, F. L., & Toppen, D. L. (1978). Kinetics and mechanism of reactions of water-soluble ferriporphyrins. 2. Reduction by ascorbic acid. *Inorganic Chemistry, 17*(1), 74–77. https://doi.org/10.1021/ic50179a016
42. Deakin, M. R., Kovach, P. M., Stutts, K. J., & Wightman, R. M. (1986). Heterogeneous mechanisms of the oxidation of catechols and ascorbic acid at carbon electrodes. *Analytical Chemistry, 58*(7), 1474–1480. https://doi.org/10.1021/ac00298a046